Integrated smart gas flow sensor with 2.6 mW total power consumption and 80 dB dynamic range

Massimo Piotto [a], Francesco Del Cesta [b], Paolo Bruschi [b]

[a] IEIIT – Pisa, CNR, via G. Caruso 16, I-56122, Pisa, Italy
[b] Dipartimento di Ingegneria dell'Informazione, University of Pisa, via G. Caruso 16, I-56122 Pisa, Italy

Corresponding author: Massimo Piotto; e-mail: massimo.piotto@ieiit.cnr.it; Tel +39 050 2217657, Fax +39 050 2217522

Abstract

A thermal flow sensor including sensing structures and a read-out interface in a single chip is proposed. The sensing structure is a microcalorimeter based on a double heater configuration while the low noise electronic interface performs signal reading and offset compensation. The device has been fabricated with a commercial CMOS process followed by a post-processing procedure. Post-processing has been customized in order to increase the thermal insulation of the sensing structures from the silicon substrate and improve the heat exchange between the sensor and the gas flow. Device characterization confirms the effectiveness of the proposed fabrication method in increasing the sensitivity at constant power consumption without affecting the dynamic range.

Keywords: thermal flow sensor; electronic interface; system-on-chip (SoC); flow sensor design; low power design.

1. Introduction

MEMS (Micro-Electro-Mechanical System) flow sensors, based on a thermal principle, allow detection of extremely small fluid flow rates with high accuracy and resolution [1-4]. Micromachining

technologies have allowed fabrication of miniaturized sensors with response times and power consumptions at least one order of magnitude lower than their macroscopic counterparts. In fact, commercial MEMS flow sensors with response times in the order of millisecond and power consumptions of a few tens of milliwatts are available [5,6]. Recently, emerging battery-powered applications, such as wireless sensor networks, wearable sensors and propulsion systems for pico-satellites, are introducing more stringent requirements in terms of power consumption. For this reason, considerable research effort is recently being spent to further reduce the power consumption of these devices. Unfortunately, reducing the power delivered to a thermal flow sensor without applying also structural improvements results in a proportional sensitivity reduction [7, 8]. As it is well known, the sensitivity is not important *per se*, but for its effects on the minimum resolvable flow rate, given by the ratio between the output peak-to-peak noise and the sensitivity. To compensate for the sensitivity degradation produced by reducing the power delivered to the sensor it is necessary to develop new sensing structures with an intrinsically higher sensitivity. This can be accomplished by using thermopiles formed by a large number of thermocouples [8] with the side-effect of increasing the sensor dimensions and, proportionally, the required heater power. It can be shown that, for a given sensor transversal dimension, the intrinsic sensor resolution is only weakly affected by the thermocouple number [9]. Temperature probes based on highly sensitive materials, like amorphous germanium thermistor [10, 11], have been proposed as an effective method to increase the overall sensitivity, allowing reduction of the power consumption down to the sub-milliwatt range. These materials are generally not fully compatible with a CMOS process, preventing the adoption of a post-processing approach and, in particular, the integration of the sensing structure and the read-out electronics into a single chip. Another commonly used approach to increase the device sensitivity without changing the power is shrinking the channel cross-section at the sensing structure location, in order to locally increase the flow velocity. However, this causes a steep increase of the flow-sensor insertion loss (pressure drop) that limit application in low-

pressure gas distribution lines. Furthermore, the maximum applicable flow, beyond which saturation of the response occurs, is adversely affected, producing a degradation of the device dynamic range (DR), defined as the ratio between the maximum and minimum detectable flow. A strategy that can be applied to decrease the power consumption preserving sensitivity and range is based on reducing the heat loss of the sensor elements toward the substrate, because only the heat exchange with the fluid contributes to the output signal. In fact, many of the proposed MEMS flow sensors consist of micro elements (heaters and temperature probes) placed on dielectric membranes suspended over a cavity etched into the silicon substrate [1-4, 7-16]. This strategy is at the basis of the devices proposed by our group so far [9, 17-19]. In this work, a novel fabrication process aimed at further increasing thermal insulation between the sensing structures and the substrate is proposed. The method exploits one of the metal layer of the CMOS process as a mask in replacement of the typical photoresist layer used to define openings in the dielectrics and then the membrane geometry. In this way, thinner dielectric membranes can be obtained, as recently demonstrated in [20], where membranes with low thermal mass were designed for acoustic applications. In this work, the method is applied for the first time to flow sensors. Furthermore, the read-out electronics has been optimized with respect to [19] in order to minimize power consumption preserving low noise performances. These research efforts have been made to obtain flow sensors with improved low power and resolution characteristics. The target is using these devices for the development of miniaturized directional anemometers based on a recently proposed approach [21] that requires detection of multiple airflows.

2. Device description and fabrication

The device has been obtained by applying a post-processing micromachining procedure to chips designed with the STMicroelectronics BCD6s (Bipolar-CMOS-DMOS, three metal layers) process. A schematic view of the sensing structure is shown in Fig. 1. The structure is a differential micro-calorimeter, consisting of two thermopiles symmetrically placed across two resistive heaters. The thermopiles are

made up of 10 *n*-polysilicon/*p*-polysilicon thermocouples with the hot contacts at the tip of a SiO_2 cantilever beam and the cold contacts on the silicon substrate. The heaters are *p*-polysilicon resistors (2 kΩ at room temperature) placed on SiO_2 membranes suspended over the cavity by means of four arms.

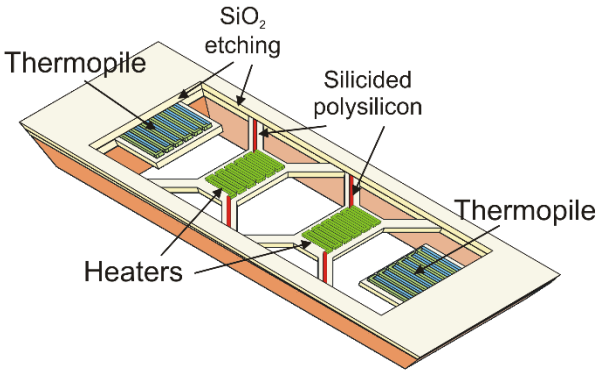

Figure 1. Perspective view of the proposed device: the two strategies to improve the thermal insulation of the membranes, i.e. silicided polysilicon interconnections and dielectric thickness reduction, are highlighted. (not to scale).

The double heater configuration has been adopted since it allows effective compensation of the sensor offset, deriving from unavoidable fabrication tolerances. The offset is cancelled by introducing a proper unbalance between the currents that feed the heaters. The advantage of this approach is that both the offset and its temperature drift are strongly reduced [18].

In order to increase the thermal insulation of the suspended membranes from the silicon substrate two strategies have been implemented. First, instead of aluminum, silicided polysilicon is used for the connections to the heaters through the suspended arms of the membranes. This material has a low enough sheet resistance to minimize unwanted power dissipation along the connecting lines, while its thermal conductivity is almost one order of magnitude lower than aluminum one. As a result, heat loss from the heaters to the substrate through the electrical interconnections can be significantly reduced using silicided polysilicon interconnections [9]. In this work, a further improvement is obtained by reducing the thickness of the SiO_2 membranes and cantilevers with respect to the total dielectric stack of the process. Thinner membranes guarantee a better thermal insulation of both the heaters and the hot contacts of the

thermopiles. In the case of the heaters, a higher overheating is obtained at the same power consumption, while for the thermopiles this means that convective heat exchange turns into greater temperature differences between the hot and cold contacts. A further advantage of reducing the thickness of the dielectrics is the better thermal contact of the sensor elements with the fluid stream. All these factors contribute to increase the overall sensitivity at constant power consumption, or, equivalently, to reduce the power consumption for a given sensitivity.

Different sensing structures have been integrated with a low power, low noise electronic interface into the chip shown in Fig. 2, where the main subsystems are highlighted. Two sensing structures have been involved in this work. The first one, named low power structure (S1), is designed and fabricated applying the two described improvements, i.e. silicided polysilicon interconnections and membrane and cantilever thickness reduction. In order to evaluate the actual improvement brought by the dielectric thickness reduction, a reference sensing structure (S2), designed to be processed with the previous version of the post-processing procedure [19], has been included into the test chip. Therefore, the reference structure differs only on the membrane and cantilever thickness. Both structures are connected to the same electronic interface through an integrated analog multiplexer. The heater driver feeds the heaters with two currents, whose differential component can be digitally tuned (10-bit resolution) to implement the mentioned drift-free cancellation of the sensor offset [18]. The thermopile differential output voltage is amplified (gain=200) by the integrated low-noise, low-power chopper amplifier (In-Amp and oscillator blocks in Fig. 2). A set of digital registers, which can be accessed by an embedded serial port, controls the interface parameters.

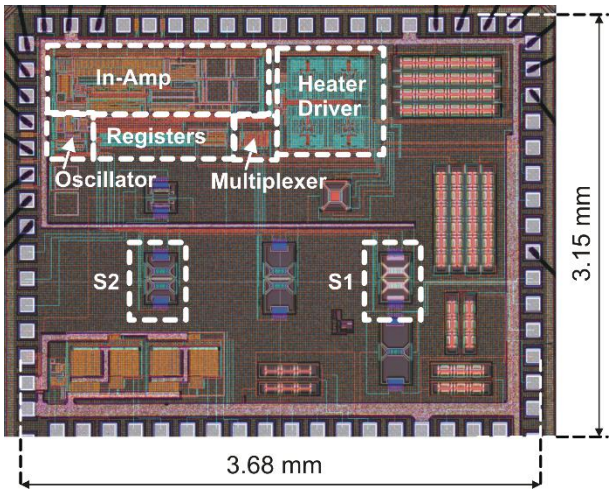

Figure 2. Chip photograph with indication of the main subsystems. Note that the chip layout has been superimposed on the optical photograph to show the electronic circuits buried under the planarization dummies.

Thermal insulation between the sensing elements and the silicon substrate is obtained by applying a post-processing procedure to the chips returned by the silicon foundry. Previous versions of the post-processing technique and related problems / solutions are described in [17, 19]. The procedure described in this work is a variant of the previous versions and requires a slightly different design of the sensing structures. This variant has been applied for the fabrication of the low power structure (S1) and the main steps are schematically shown in the left part of Fig. 3. The rectangular membranes and the cantilevers are defined using the second metal layer (Metal 2) of the BCD6s process flow, exploiting the selectivity of the SiO_2 etch in CF_4 plasma towards aluminum. The metal mask is aligned to the thermopiles and the heaters during the chip design (Fig 3a). In this way, all the dielectric layers above the Metal 2 are removed during the SiO_2 etch (Fig. 3b) reducing the thickness of the suspended dielectric membranes. Note that the passivation layer over the sensor areas was removed by the silicon foundry before the post-processing, as shown in Fig. 3a.

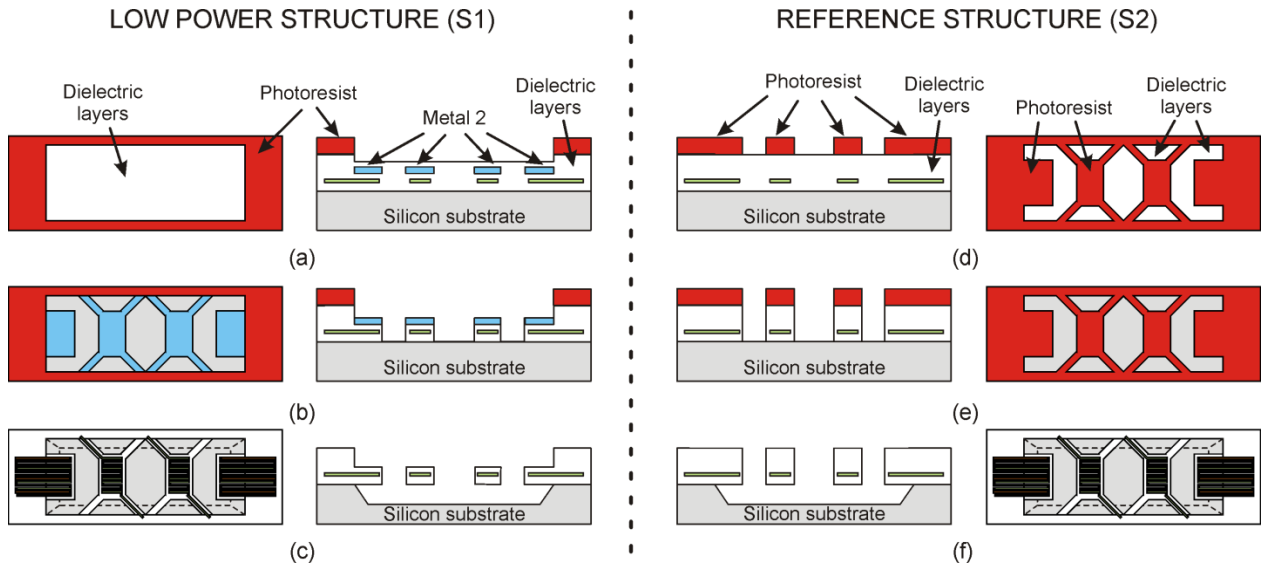

Figure 3. Cross section and plan view of the two different sensing structures during the main steps of the fabrication process. Left: low power structure (S1) (a) prior to reactive ion etching (RIE) in CF_4 (b) after the RIE and (c) after the Metal 2 removal and TMAH etching. Right: reference sensing structure (S2) (d) prior to reactive ion etching (RIE) in CF_4 (e) after the RIE and (f) after the TMAH etching. (not to scale).

An 8 μm thick photoresist film (MEGAPOSIT™ SPR™ 220-7.0) has been used only to roughly define the sensor areas, protecting the rest of the chip and the bonding pads from the subsequent Reactive Ion Etching (RIE) (Figs 3a and 3b). As far as the reference structure is concerned, the same photoresist film has been used to define the geometries of the membranes by means of a photomask, as schematically shown in the right part of Fig. 3, following a procedure similar to that reported in [17, 19]. Furthermore, the Metal 2 layer is not present and the passivation layer is not removed by the silicon foundry (Fig 3d). The RIE was performed in CF_4/Ar (50%/50%) gas mixture with a RF power of 100 W (Fig. 3b and Fig. 3e). After the RIE, the metal mask has been removed with a H_3PO_4–HNO_3–CH_3COOH water mixture at 45 °C using the photoresist layer as pad protection. Then photoresist has been removed with acetone at room temperature and the silicon substrate has been anisotropically etched for 150 minutes at 85 °C in a solution of 100 g of 5 wt% TMAH with 2.5 g of silicic acid and 0.7 g of ammonium persulfate, as schematically shown in Fig. 3c and Fig. 3f. Due to the fast degradation of the TMAH solution [17], the

silicon etching has been performed in three separate 50 minutes long steps, each one performed with fresh reagents. Investigations performed with the Scanning Electron Microscope showed that, for both the low power and reference structure, mechanical deformation (e.g. bending) of the membranes did not occur, proving that residual stress was not an issue for the proposed fabrication technique.

3. Device characterization

The chips were glued to ceramic DIL 28 packages and a purposely-built package based on a PMMA (Poly-methyl-methacrylate) gas conveyor [17, 19] was applied to the chip surface, obtaining the structure shown in Fig. 4. Note that the sensing structure is included into a flow channel with a 0.5 × 0.5 mm^2 cross section and two stainless steel needles are used for gas inlet and outlet. The device has been connected to a gas line equipped with a reference mass flow controller (MKS 1179B).

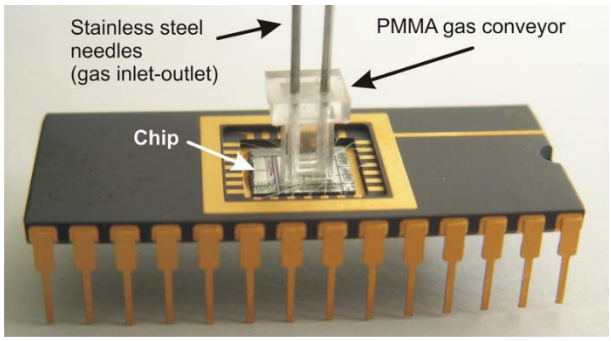

Figure 4. Photograph of the final device after the application of the PMMA gas conveyor.

The response of the low power sensing structure (S1 in Fig 2) to a nitrogen flow in the ± 100 sccm range is shown in Fig. 5a. The amplifier output voltage is read by a microcontroller board equipped with high-resolution analog-to-digital converters. The signal bandwidth is digitally limited to 10 Hz. The sensitivity for small flows was estimated from a linear fit performed in the dashed box shown in the figure (±2 sccm interval), obtaining a value of 13.2 mV/sccm. A time diagram of the output noise, measured in condition

of zero flow, is shown in Fig. 5b. In order to avoid interference from micro-flows induced into the sensor channel by possible pressure fluctuations along the measurement line, the sensor was disconnected from the line and placed into a metal box that provided also shielding from electro-magnetic interference. In addition to a very small offset component (nearly 40 μV), a peak-to peak noise magnitude of nearly 0.12 mV can be estimated from Fig. 5b. Measurements performed with short-circuited amplifier input terminals showed that the amplifier contribution to the total noise is less than 15 %. It can be argued that, similarly to [19], the noise is practically due to only the output Johnson noise of the thermopiles. Dividing the noise level by the sensitivity, a resolution of nearly 0.009 sccm, corresponding to a gas velocity in the channel of nearly 0.6 mm/s, can be estimated. Considering that the response is still monotonic up to flow rates of ± 100 sccm, the dynamic range, given by the ratio of the maximum flow rate to the resolution, is nearly 81 dB, corresponding to more than 4 decades. Note that the sensitivity and then the resolution progressively get worse at high flow rates.

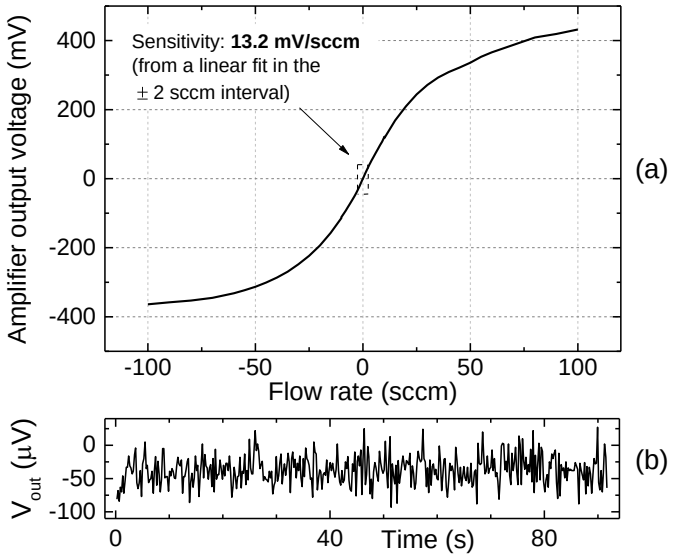

Figure 5. (a) Response of the low power sensing structure (S1) to a nitrogen flow. The amplifier output voltage (gain=200) is shown. Negative flows are obtained by swapping the inlet and outlet connections. The dashed box indicates the region where the sensitivity was estimated. (b) Time diagram of the output noise in zero flow condition.

The difference between the response to positive and negative flows, which is particularly noticeable at higher flow rates, was observed also in single heater sensing structures [9]. This suggests that this phenomenon is not tied to the unbalanced currents applied to the two heaters to compensate the offset. A possible cause is the asymmetry of the flow channel deriving from the relatively large tolerances of the procedures used to fabricate and align the gas conveyor on the chip surface.

The measurements in Fig. 5a and 5b were performed setting the current of both heaters to around 0.3 mA, with a small differential component applied to reduce the output offset [18] to the same level as the output noise. With these settings, the power delivered to each heater was 0.21 mW, while the total current absorption of the chip, including the electronic interface, is 0.8 mA. This, at a supply voltage of 3.3 V, corresponds to a total power consumption of 2.6 mW. The resolution by power-consumption product is 1.56 mW×mm/s, nearly three time higher (i.e. worse) than the sensors in [10], where, on the other hand, the amplifier supply current was not taken into account and a much smaller DR (26 dB) can be calculated from the reported data. It should be observed that the DR of the proposed sensor was extrapolated considering that a linear response is maintained at extremely low flow velocities. Due to limitations of the experimental apparatus, the linearity was confirmed down to 0.1 sccm (~6 mm/s). Further investigation is required to exclude the occurrence of threshold phenomena due to natural convection [10].

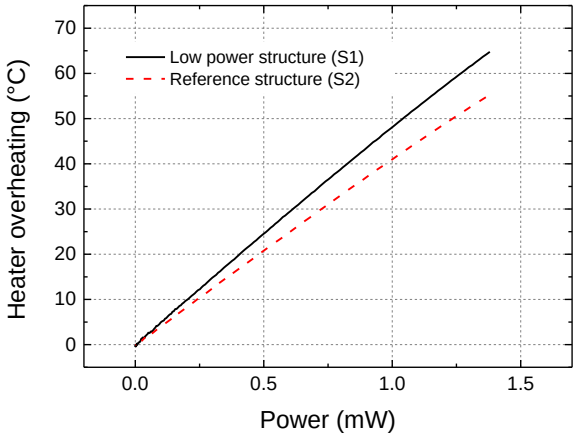

Figure 6. Heater overheating as a function of power for the low power structure (S1 in Fig. 2) and the reference one (S2 in Fig. 2).

In order to evaluate the actual improvement brought by the dielectric thickness reduction, the low power structure has been compared with the reference sensing structure (S2 in Fig. 2) that differs only on the membrane and cantilever thickness. First, the effects on the heater thermal insulations have been evaluated measuring the heater overheating as a function of power. The test was performed by delivering the same current to both heaters by means of an external parameter analyzer (HP 4145B). Fig. 6 shows the overheating as a function of the power delivered to a single heater. As expected, a nearly linear behavior has been obtained in both cases but the low power structure (S1) reaches higher temperatures for the same power levels. This means that thermal insulation of the heater from the silicon substrate has been increased. In fact, a thermal resistance of 49.0 x 10^3 K/W has been calculated from this data for the heater with the thinner membrane while the heater of the reference structure presents a thermal resistance of 40.5 x 10^3 K/W. The modest improvement of the thermal insulation (nearly 21%), obtained with an estimated membrane thickness reduction of more than 50 %, is justified by the fact that thermal conduction through the dielectrics is only one of the various contributions to the total heat drainage. Important contributions come also from the electrical interconnections (silicides) and conduction through the air gaps, which are left unchanged with respect to the reference structure.

On the other hand, the improvements in terms of sensitivity are much more pronounced, as demonstrated by Fig.7, where the responses to nitrogen flows of the low power and reference structures are compared. In this experiment, the two structures are driven with identical heater powers (0.6 mW), nearly three times the value used in the experiment of Fig.5. The structures, belonging to the same test chip, are packaged using a dual flow conveyor to form two independent flow channels [9]. The channel cross section at the sensing structure location is identical for the two devices. The measurements, performed in the low flow regime, show that the sensitivity improvement obtained with the membrane thickness reduction is close to 100 %. Since the heater temperature is increased only by 21 %, the improvement should be ascribed mostly to a more efficient heat exchange between the sensor elements and the gas flow, as anticipated in previous section.

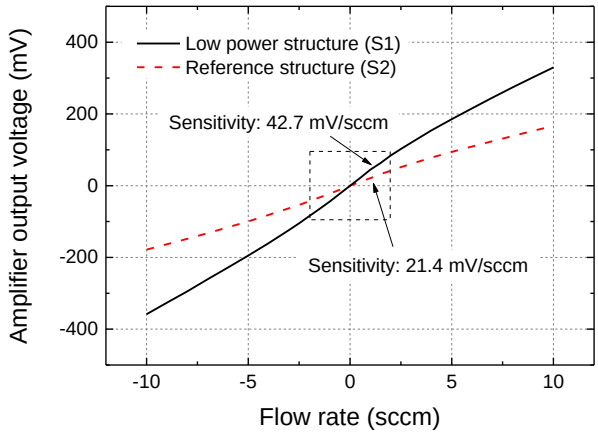

Figure 7. Response of the two sensing structures (S1 and S2 in Fig. 2) to a nitrogen flow; the heaters of the two structures were driven with the same power (P = 0.6 mW). Negative flows are obtained by swapping the inlet and outlet connections. Sensitivities are estimated with a linear fit performed in the [-2 sccm, 2 sccm] interval.

The sensitivity ratio between the improved and reference structure is maintained at different power levels. The comparison shown in Fig. 7 has been performed at an increased power level with respect to the experiment of Fig. 5 to show the possibility of modulating the sensitivity by changing the heater current.

The integrated interface allows selection of three different current magnitudes corresponding to three different power dissipation / sensitivity trade-offs.

4. Conclusions

A single-chip, multichannel flow sensor including both the sensing elements and the electronic interface has been presented. The chip, which is an evolution of a recently presented device, has been fabricated applying a custom post-processing technique to an integrated circuit, produced with a commercial microelectronic process (BCD6s of STMicroelectronics). The major innovation with respect to the previous device is the use of a metal layer of the original BCD6s process as a mask for the RIE etching. This layer, being embedded into the dielectrics, allows reduction of the final membrane thickness with respect to standard post-processing techniques relying on a photoresist mask deposited on top of the full dielectric stack. The resulting sensitivity increase of nearly 100 %, and the low noise characteristics of the integrated interface allowed the fabrication of a flow sensing platform with unique dynamic range / power consumption combination. In particular, a dynamic range of four decades has been achieved with a power consumption of 2.6 mW, which is significantly lower than that reported for most calorimetric flow sensors proposed in the literature (see the review [4]). The exception is given by Ref. [10], where a power-resolution product nearly three times lower is reported but with a significantly smaller dynamic range. The sensor response is slightly dependent on the direction of flow, especially in the region of high flow rates where a significant non-linearity is present. This phenomenon, which was ascribed to asymmetries in the channel geometry and sensing structure placement, imposes individual calibration of the sensors, using different parameters for the negative and positive flow rate interval. Adoption of improved techniques for the fabrication and alignment of the gas conveyor can be a viable strategy to reduce the response asymmetry.

References

[1] B.W. van Oudheusden, Sens. Actuators A: Phys. 30 (1992) 5–26.

[2] N. T. Nguyen, Flow Meas. Instrum. 8 (1997) 7-16.

[3] Y.-H. Wang, C.-P. Chen, C.-M. Chang, C.-P. Lin, C.-H. Lin, L.-M. Fu, C.-Y. Lee, Microfluid Nanofluid 6 (2009) 333-346.

[4] J. T. W. Kuo, L. Yu, E. Meng, Micromachines 3 (2012) 550-573.

[5] Sensirion Online Product Catalog, [Online]. Available: http://www.sensirion.com/.

[6] Honeywell Online Product Catalog, [Online]. Available: http://sensing.honeywell.com/.

[7] T.S.J. Lammerink, N.R. Tas, M. Elwenspoek, J.H.J. Fluitman, Sens. Actuators A 37–38 (1993) 45-50.

[8] S.-C. Roh, Y.-M. Choi, S.-Y. Kim, Sensors and Actuators A 128 (2006) 1-6.

[9] P. Bruschi, M. Piotto, Micromachines 3 (2012), 295-314.

[10] A. S. Cubukcu, E. Zernickel, U. Buerklin, G. A. Urban, Sensors and Actuators A: Physical 163 (2010) 449–456.

[11] S. Cerimovic, A. Talic, T. Sauter, F. Kohl, R. Beigelbeck, J. Schalko, A. Jachimowicz, Proceedings of IEEE Sensors 2009, Christchurch, New Zealand, pp. 1325-1328.

[12] B.W. van Oudheusden, A.W. van Herwaarden, Sens. Actuators A21-A23 (1990) 425-430.

[13] D. Moser, R. Lenggenhager, G. Wachutka, H. Baltes, Sensors and Actuators B 6 (1992) 165-169.

[14] M. Dijkstra, M.J. de Boer, J.W. Berenschot, T.S.J. Lammerink, R.J. Wiegerink, M. Elwenspoek, Sensors and Actuators A 143 (2008) 1-6.

[15] M. Ashauer, H. Glosch, F. Hedrich, N. Hey, H. Sandmaier, W. Lang, Sensors and Actuators 73 (1999) 7-13.

[16] A. Glaninger, A. Jachimowicz, F. Kohl, R. Chabicovsky , G. Urban, Sensors and Actuators 85 (2000) 139-146

[17] P. Bruschi, M. Piotto, N. Bacci, Microelectronics Journal 40 (2009) 1300-1307.

[18] P. Bruschi, M. Dei, M. Piotto, IEEE Sensors Journal 11 (2011) 1162-1167.

[19] M. Piotto, M. Dei F. Butti G. Pennelli, P. Bruschi, IEEE Sensors Journal 12 (2012) 3309-3317.

[20] M. Piotto, F. Butti, E. Zanetti, A. Di Pancrazio, G. Iannaccone, P. Bruschi, Sensors and Actuators A 229 (2015) 192-202.

[21] M. Piotto, G. Pennelli, P. Bruschi, Microelectronic Engineering, 88 (2011) 2214–2217.